2022 44th Annual International Conference of
the IEEE Engineering in Medicine & Biology Society (EMBC)
Scottish Event Campus, Glasgow, UK, July 11-15, 2022

2022 44th Annual International Conference of the IEEE Engineering in Medicine & Biology Society (EMBC) | 978-1-7281-2782-8/22/$31.00 ©2022 IEEE | DOI: 10.1109/EMBC48229.2022.9871297

AEPUS: a tool for the Automated Extraction of Pennation angles in Ultrasound images with low Signal-to-noise ratio for plane-wave imaging

S. Vostrikov[1], A. Cossettini[1], C. Leitner[2], C. Baumgartner[2], L. Benini[1,3]

***Abstract*— The penetrating ability of ultrasound (US) combined with its real-time operation make it the perfect tool for investigating muscle contraction mechanics during complex functional tasks, e.g., locomotion.**

Changes in fascicle lengths and pennation angles of muscle fascicles strongly correlate with the capacity of skeletal muscles to produce forces, thereby represent fundamental parameters to be tracked. While the gold standard for extracting these features from US images is still based on manual annotation, the availability of recording devices capable of generating big data of muscle dynamics makes such manual approach unfeasible, setting the need for automated muscle images annotation tools.

Existing approaches, however, are seriously limited, also in view of the continuous developments and technology advancements for ultrafast US and plane-wave imaging. In fact, they rely on conventional (slow) B-mode imaging, make use of point tracking approaches (which often fail due to out-of-plane motion), or can only operate on very high quality images. To overcome all these limitations, we present AEPUS, an automated image labeling tool capable of extracting pennation angles from low quality images using a very small number of plane waves, therefore making it capable of exploiting all the benefits of ultrafast US.

***Clinical relevance*— Ultrasound is a standard research tool to investigate alterations of spastic muscles in children with Cerebral Palsy. We propose a reliable and time-efficient method to track muscle features in ultrasound images and support clinical biomechanists in their analyses.**

I. Introduction

Ultrasound (US) is a compact, non-invasive and recognized tool to study human musculoskeletal functions in-vivo [1]. With the help of US, muscle mechanics can be observed in real-time, during complex functional tasks. For example, biomechanical studies on muscles observe pennation angles and fascicles lengths to conclude on force production capacities [2]. In fact, in clinical populations, knowledge about their alterations due to short or long-term treatments can be crucial for developing new therapeutic strategies [3].

The extraction of these muscle features from US images requires labor-intensive manual labeling. Hence, accurate automated approaches are needed to process longer sequences of images. Such tools can significantly reduce the processing time and subjectivity of the results compared to a single manual annotation [4], and to address this need, multiple image analysis approaches have been proposed [5].

One common strategy to measure pennation angles makes use of feature tracking algorithms, which track the positions of fascicle's sections through image sequences. Particularly, the Lucas–Kanade optical flow algorithm is widely used to track the manually marked fascicle's end points [6], [7], thereby obtaining an estimation of the fascicle orientation over time. However, these methods have multiple drawbacks. First, tracking methods require the consistent presence of the key tracked points in all consecutive frames. Therefore, the accuracy of the tracking is influenced by out-of-plane movements of the muscle fibers, that naturally occur during muscle contraction. Moreover, such approaches rely on the assumption of slow displacement of the key tracked point position between consecutive frames. Hence, they require very high frame rates to track fast muscle movements. Finally, the tracking errors of the individual frames accumulate over time, causing temporal drift. While some tools (such as Ultratrack [8]) implement correction algorithms, manual adjustments are still often required to get good results. Thus, the application of tracking-based algorithms for image analysis of high frame rate sequences still faces important limitations.

An alternative strategy to identify pennation angles is offered by structure-based algorithms sensitive to the parallel arrangement of the muscle fibers, that appear in the US images as bright, coherently oriented lines. In [9], [10], the Hough transform was employed to recognize the line objects by identifying the fascicle edges and grouping them. However, this approach relies on the edge map, that cannot be easily extracted unless US images have a high signal-to-noise ratio (SNR). As an alternative, the Radon transform (RT) can be directly applied to the greyscale image, and it also allows to detect linear features in the US B-mode scans. In fact, lines in the image appear as peaks in the sinogram (Radon space) [11], from which the positions of the individual fascicles can be identified [12], and by applying maximum variance criteria the dominant orientation of the fibers can also be computed (see Fig. 6 of [10]). Being the result of an integral transform, the sinogram is less susceptible to noise, although some studies proposed to use additional image enhancing techniques (e.g., vessel enhancement filters [13]) before calculating the transformation.

This work was supported by the Swiss National Science Foundation (Project PEDESITE) under grant agreement 193813.

[1]Department of Information Technology and Electrical Engineering, ETH Zürich, Zürich, Switzerland {vsergei, cossettini.andrea, lbenini}@iis.ee.ethz.ch

[2]Institute of Health Care Engineering, TU Graz, Graz, Austria {christoph.leitner, christian.baumgartner}@tugraz.at

[3]Department of Electrical, Electronic and Information Engineering "Guglielmo Marconi" (DEI), University of Bologna, Bologna, Italy luca.benini@unibo.it

All the approaches mentioned above rely on the conventional focused B-mode US imaging modality, that has a fundamentally limited frame rate (FR). In fact, assuming the speed of sound of 1540 m/s, 5 cm imaging depth and 128 transmission beams, the maximum achievable frame rate is 120 FPS. However, recent studies demonstrated the need for much higher FR ($>$ 150 Hz) to capture muscles and tendons in motion [14]. Going beyond the classical US modalities, we can employ ultrafast plane wave (PW) imaging [15] to transmit unfocused waves and obtain a higher FR. More precisely, for similar image quality, plane wave transmissions and coherent compounding can provide a 10$\times$ increase in the frame rate compared to the conventional scanning technique [16]. In addition to using PW modality, the number of required transmissions per frame should also be optimized to decrease the data rate and reduce the hardware requirements for the US system. However, none of the existing image processing algorithms are tailored to operate on US images captured in PW mode, and the question on the optimal number of transmissions remains open.

In this work, we present AEPUS, a tool for the extraction of pennation angles that works with low-quality (low-SNR) US images captured with plane wave modality reaching roughly $\pm 2.6^\circ$ accuracy compared to manual annotations when using only 3 unfocused transmissions (PW3) per frame. The method independently processes each image (thus, overcoming the limitations of tracking-based approaches), works in PW mode (thus, it is compatible with ultrafast US applications), and requires only a minimal number of parameters to be tuned. In the following, we describe the algorithm, compare it with manually annotated data, and discuss how the number of plane waves influences the accuracy of the proposed approach.

II. Algorithm

To help the detection of pennation angles, prior knowledge on muscle physiology can be leveraged. Muscle fibers are located in between the deep and superficial aponeuroses, that usually have a very high brightness compared to the individual fascicles (Fig. 1). Hence, the first step of the algorithm consists in identifying the aponeuroses and the region of the image containing the fascicles is identified. Finally, the average pennation angle of the muscle fibers can be measured in such region. The Radon transform (RT) represents the main tool to achieve these goals, and for the sake of a self-contained paper, we also include a primer on its working principle.

A. Radon Transform

The Radon transform is defined as the integral of the image intensity $I(x, y)$ along a line parametrized by the distance s from the origin of the image (conventionally set at the center of the image) and the inclination angle ϕ relative to the x-axis, that corresponds to:

$$Rf(\phi, s) = \iint I(x, y)\, \delta(s - xsin\phi - ycos\phi)\, dxdy \quad (1)$$

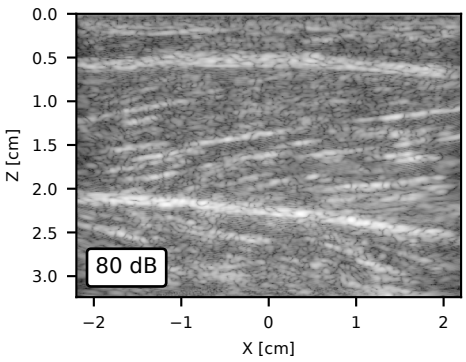

Fig. 1. Original US image of a Gastrocnemius lateralis muscle captured with 15 plane waves (max. angle 15°).

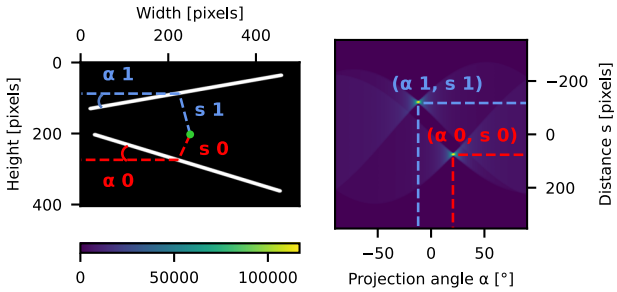

Fig. 2. An example binary image with two lines (left) and its radon transform (right). The green point represents the center of the image that is the origin of radon transform.

The Radon-transformed image is called sinogram and is represented in the (α, s) variables. For convenience, in the subsequent sections we will use the Radon transform $Rf(\alpha, s)$ with $\alpha = \phi - \pi/2$, so as to keep the projection angle in a range $[-\pi/2, +\pi/2]$.

Because of the Dirac delta function δ under the integral, a line with parameters s^*, ϕ^* in the image domain produces a peak at the coordinates $s = s^*$ and $\phi = \phi^*$ in the RT space. Fig. 2 shows a simple example of such phenomenon, where two lines with inclination α_0 and α_1 and distance from the origin s_0 and s_1 appear as peaks at the sinogram coordinates (α_0, s_0) and (α_1, s_1). From an user's perspective, the Radon transform can be seen as a line-to-peak converter, where the intensity of the peaks are determined by the summation of the values of the pixels along the selected line in the original image.

B. Detection of the superficial and deep aponeuroses

The proposed algorithm starts with the identification of deep and superficial aponeuroses in the US image. As these structures appear as highly reflective lines, applying a RT on the original image makes them appear as peaks in the Radon space (Fig. 3).

Extracting these peaks can be challenging, since the rectangular shape of the US image also transforms into a non-flat surface in the Radon space (Fig. 4). Therefore, Fig. 3 mixes both the information about the structures (aponeuroses, fascicles) contained in the image, and the information about the shape (edges) of the image itself. To accurately find the

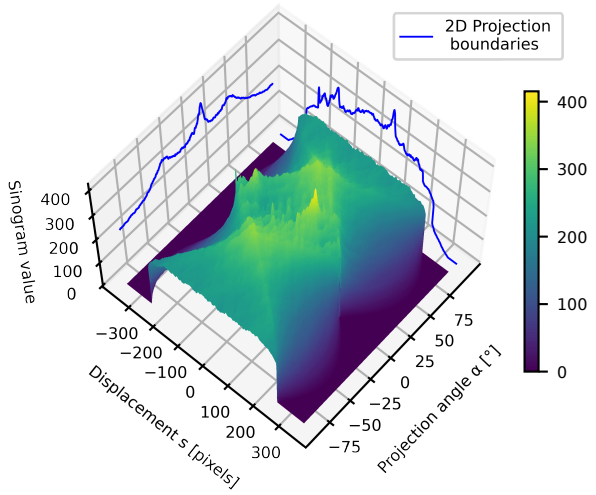

Fig. 3. Sinogram of the original US image

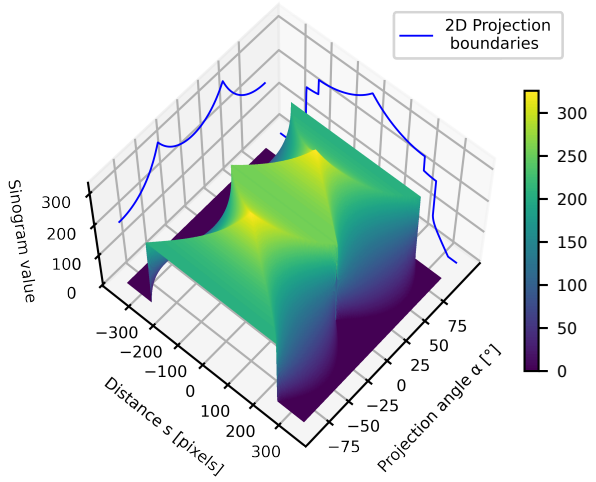

Fig. 4. Sinogram of an uniform rectangular US image, whose pixels have the same value. When used to compensate the shape-induced artifact, the value of the pixels is set equal to the mean brightness of the enhanced image (see main text and Fig. 5).

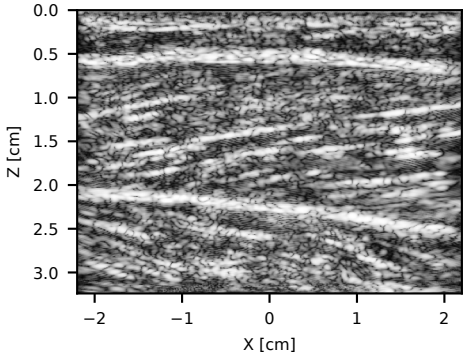

Fig. 5. Contrast Limited Adaptive Histogram Equalization enhancement of the US image of Fig. 1.

displacements and inclination angles of the aponeuroses, we should compensate for this shape-induced artifact.

Another factor affecting the Radon transform is the attenuation of ultrasound signals with the depth. In fact, imperfect time gain compensation (TGC) creates a brightness gradient in the US image along Z axis, which results in an inclined surface in the Radon space.

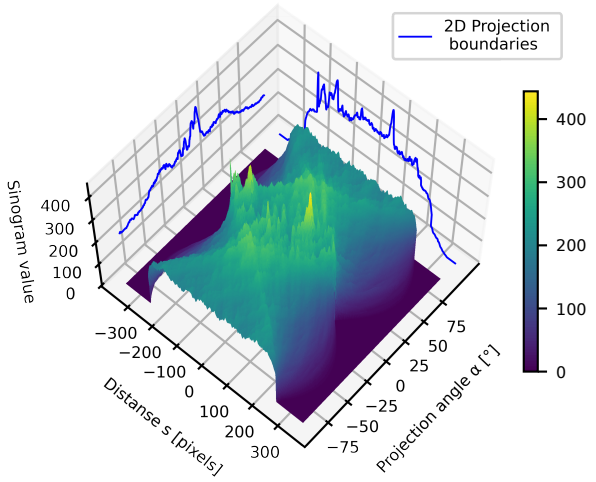

Fig. 6. Sinogram of the enhanced US image (of Fig. 5). The peaks representing the aponeuroses are more pronounced compared to the sinogram of the original image (see Fig. 3).

To mitigate for these two non-idealities and identify the aponeuroses, we proceed as follows:

- We compensate the imperfect TGC by applying a Contrast Limited Adaptive Histogram Equalization (CLAHE) [17] on the original image (shown in Fig. 1) to redistribute the lightness values. Fig. 5 shows the resulting enhanced US image.
- We calculate the mean pixel brightness value of the enhanced image of Fig. 5.
- We generate an uniform image that has the same resolution (number of pixels) as the original image, and whose pixels have all the same value equal to the mean brightness calculated at the step above.
- We calculate the RT of such uniform image. Fig. 4 shows the corresponding sinogram.
- We calculate the RT of the enhanced image of Fig. 5. Fig. 6 shows the corresponding sinogram.
- We subtract the sinogram of the uniform image from the sinogram of the enhanced image. Fig. 7 shows the corresponding sinogram. The resulting surface has two distinguished peaks (deep and superficial aponeuroses).
- We extract the positions of the peaks. Their coordinates encode the inclination angle and displacements (relative to the image's center) of two lines which represent the aponeuroses.

Fig. 8 shows the visualization of the result on the original image.

C. Identification of the pennation angle

Fig. 9 shows the main steps for the identification of the pennation angle. After locating the aponeuroses, we apply a mask and analyze the fascicle area independently (Fig. 9 (a)). As muscle fibers appear in the US images as inclined lines, once again we make use of the RT to detect them.

However, compared to the aponeuroses, the brightness of the fascicles in the US image is much smaller. Therefore, their RT is even more affected by the imperfect TGC, the artifact of the shape of the image, and local brightness

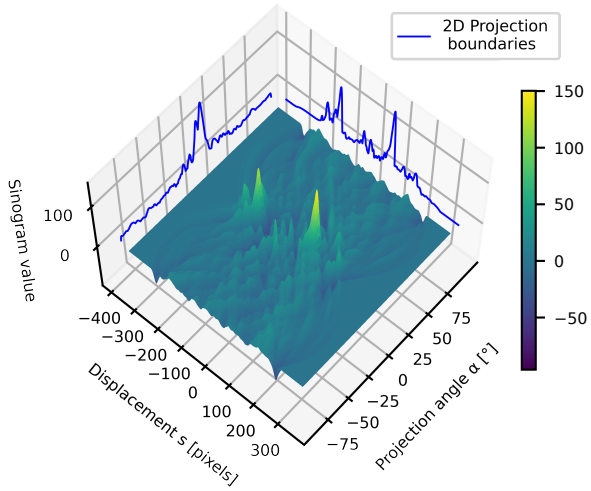

Fig. 7. Compensated sinogram of the US image, obtained by subtracting the sinogram of the uniform image (Fig. 4) from the sinogram of the enhanced image (Fig. 6). The two peaks for deep and superficial aponeuroses are clearly visible.

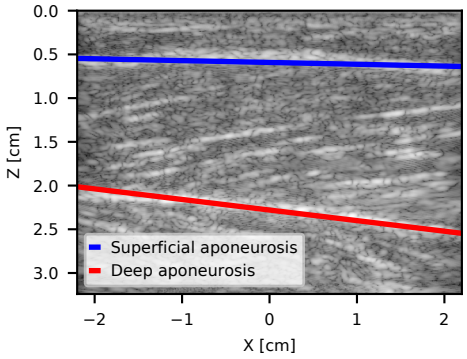

Fig. 8. Original image annotated by the aponeurosis detection algorithm.

variations. To compensate for these factors, we propose the following steps.

*1) **Generation of the compensated sinogram**:*

- We apply a mask (based on the extracted aponeuroses) on the original image (Fig. 9 (a)). We call the resulting image "fascicle image".
- The fascicle image is enhanced by the CLAHE to compensate for tissue attenuation and improve the local contrast.
- Multiple overlapping circles are inscribed into the trapezoid fascicle region to densely cover the area of interest. Fig. 9(b) shows an example of three inscribed circles. Each circle defines a region of interest (ROI) that we process independently as an individual subimage (Fig. 9(c)).
- We calculate the RT of the ROI sub-image. The circular shape of the ROI was selected due to the smoothness of its border and rotation invariance, properties that result into a smooth surface of the RT. Fig. 9(d) shows the corresponding sinogram.
- We blur the subimage of Fig. 9 with a Gaussian kernel, so that the fascicles are hardly visible. Fig. 9 (e) shows the blurred image.
- We calculate the RT of the blurred sub-image. Fig. 9 (f) shows the corresponding sinogram.
- We compensate the sinogram of the original sub-image (Fig. 9) by subtracting from it the sinogram of the blurred sub-image (Fig. 9). Fig. 9 (g) shows the resulting compensated sinogram.

The reason for blurring with a Gaussian kernel is because such a kernel acts as a low-pass filter that doesn't create a "ringing" effect. By adding this modification, we also remove the local image brightness variations within the disk area. As a result, the shape-compensated RT has nearly zero mean value and well pronounced peaks.

*2) **Identification of fascicle inclination in each ROI**:* The criteria of the maximum variance of the projection is widely used to identify the average inclination angle of the fascicles [13]. This approach works well in high-SNR scenarios (where fascicles are well pronounced and oriented in the same direction). However, during active movements, fascicles can partially disappear from the 2D plane of the US scanner (due to contractions or out-of-plane movement). Moreover, neighbor fibers can have slightly different pennation angles. All these factors lead to an inaccurate output of algorithm if relying on maximum variance criteria.

To overcome this issue, we propose the following steps.

Step 1. For each ROI, calculate the energy profile $E(\alpha)$ of its compensated sinogram:

$$E(\alpha) = \sum_{s} \left(Rf(\alpha, s)\right)^2 \tag{2}$$

where α is the projection angle, s is the displacement of the projection line from the image's center, and $Rf(\alpha, s)$ is the intensity of the sinogram. The red, purple, and blue curves in Fig. 9(h) are the energy profiles of three different ROIs.

Assuming to be in presence of a single line with inclination angle α_0 crossing the ROI, such line would appear as a symmetric peak in the radon space because of the projection symmetry. Therefore, if multiple parallel lines are presented in the subimage, the energy $E(\alpha)$ is also expected to be symmetric.

Step 2. Sum together the energy profiles of all ROIs.

Step 3. Fit a Gaussian-based symmetric function f to the $E(\alpha)$ curve of the above calculated sum, where the f function is defined as:

$$f(\alpha, \alpha_0, E_0, E_1, \sigma) = E_0 \cdot exp(-\frac{(\alpha - \alpha_0)^2}{2 \cdot \sigma^2}) + E_1 \tag{3}$$

where α_0 is the mean, E_0 is the amplitude, σ^2 is variance of the Gaussian, α is the projection angle, and E_1 is the vertical offset.

Step 4. Calculate the mean value of the sum of the fitted functions. The green line in Fig. 9(h) represents such mean value.

This value is our estimation of the fascicle inclination angle of the brightest fibers presented in the ROIs. Fig. 9(i) visualizes the result on the original image.

It is worth noticing that, in contrast to the position of the maximum value, the fitted mean accounts for the shape of the $E(\alpha)$ peak, thereby accumulating information from more

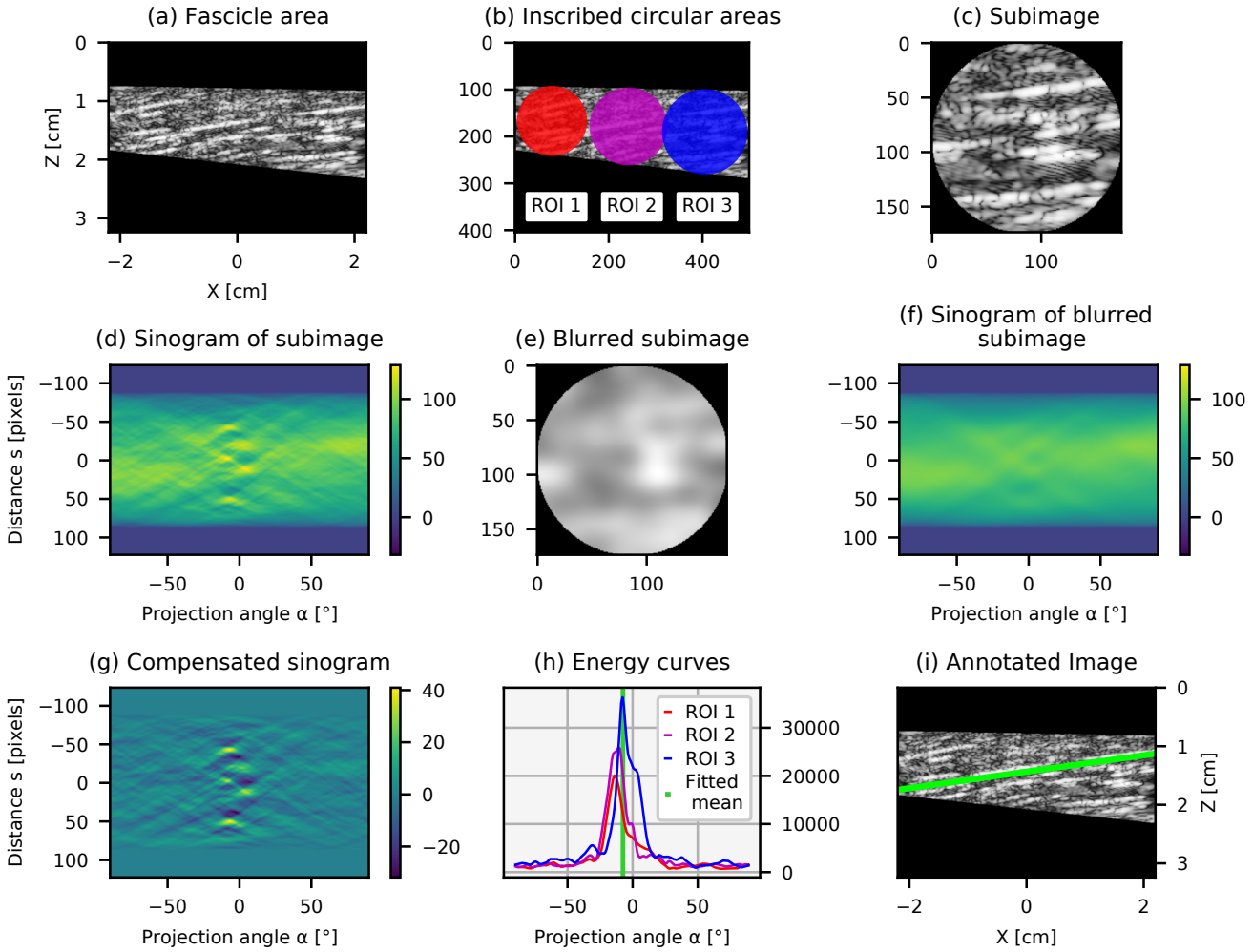

Fig. 9. Main steps of the pennation angle measurement algorithm. **(a)** Masking of the US image to isolate the fascicle area. **(b)** Inscription of multiple overlapping circles (only three circles shown for simplicity) into the masked image (a), defining ROIs that are later processed independently. **(c)** Sample subimage of one of the ROIs in (b). **(d)** Sinogram of the subimage (c). **(e)** Bluring of the original subimage (c) with a Gaussian kernel. **(f)** Sinogram of the blurred subimage (e). **(g)** Compensated sinogram of the subimage, obtained by subtracting the sinogram of the blurred subimage (f) to the sinogram of the original subimage (d). **(h)** Energy curves of the compensated sinogram (g) as a function of the projection angle for different ROIs (displayed only for three ROIs for simplicity). The green line indicates the fitted mean value. **(i)** the original image (a) is annotated with the information of the filtered mean calculated on (h).

pixels representing the fascicle in the image. Consequently, the proposed approach gives a more smooth estimation of the inclination angle in the time domain. Furthermore, instead of averaging the fitted mean values of the individual ROIs, the choice to first sum up the energy curves for multiple ROIs, applying only afterwards the f curve fitting, is done to improve the robustness to out-of-plane movements of the fascicles.

III. Experimental Verification Methodology

To test the proposed algorithm under real conditions and identify its accuracy, we collected different datasets of muscle contractions in lower limbs captured with multiple PW modality.

A. Description of the experimental protocol

A single healthy proband performed standing calf raises (Fig. 10) by doing slow, smooth, and controlled movements. This particular exercise was selected to provide largest possible variations of the pennation angle during the acquisition.

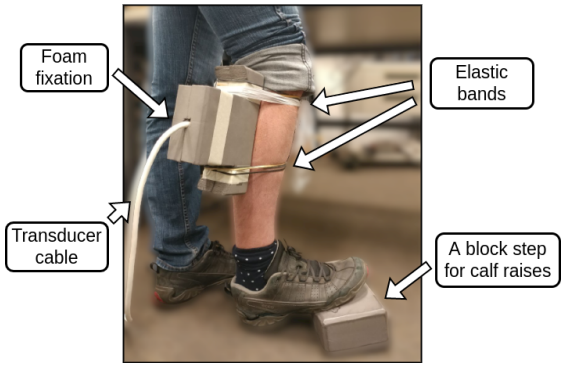

Fig. 10. Photo of the positioning of the US probe on the proband, while performing controlled calf raises exercises.

A linear array US probe (Ge-9LD, General Electric Healthcare, Chicago, IL, USA) was attached to the lateral head of the Gastrocnemius muscle. For a proper attachment of the US probe to the skin surface, we integrated the transducer into a custom-made foam fixation, which is kept

in position by elastic bands. The position of the array was adjusted to minimize out-of-plane movements and maximize the visibility of the aponeuroses and fascicles as indicated in Fig. 3 of [5].

The probe was connected to a Verasonics Vantage 256 (Verasonics, Kirkland, WA, USA) research Ultrasound system. The platform was programmed to emit 15 plane waves per frame with a maximum inclination angle of 15 degrees and capture 10 seconds of muscle contractions. The data acquisition frame rate was limited to 15 FPS during the measurements.

All the experimental procedures presented in this paper followed the principles outlined in the Helsinki Declaration of 1975, as revised in 2000.

B. Description of the dataset

In total, we made 10 data capturing sessions, each time removing and repositioning the transducer in between the sessions. Overall, we collected 1500 individual frames (150 per session), each comprising 15 independent plane wave acquisitions. For each acquisition, we used a custom implementation of the Delay-and-Sum beamformer [18] to reconstruct the images and store it in the IQ format. Subsequently, pre-beamformed data were coherently compounded into high-resolution images for testing the algorithm.

A single imaging sequence for the typical capturing session was manually annotated by an expert (who investigated muscles and tendons in 6 US studies in the past 2 years) with a cloud-based tool (Labelbox Inc., San Francisco, CA, USA). To better generalize the results, the expert inspected all sessions to choose the most representative one for performing the annotations. The original order of the images was randomly permuted to avoid the bias in the annotations caused by the previous frame. Then, the expert indicated the aponeuroses and two individual fascicles in distal and proximal areas (ROI 1 and ROI 3 in Fig. 9(b)) of each frame.

IV. Results and Discussion

In-vivo evaluations of the aponeuroses' detection show a good agreement between the proposed algorithm and the manually annotated data (Fig. 11). More precisely, the Z-position of the deep aponeurosis matches the manually annotated labels with ± 3.4 pixels accuracy (two standard deviations of the signals' difference). At the same time, the proposed approach gives an unbiased estimation of the aponeuroses inclination angle with a smaller variance compared to the manual annotation (see Fig. 11).

Regarding the fascicles, both manually and automatically extracted data curves properly capture the temporal dynamic of two consecutive muscle contractions presented in the dataset (Fig. 12). However, manually annotated inclination angles for distal and proximal areas are characterized by different mean values and high standard deviations (STD of 1.53° and 1.88° for distal and proximal, respectively; see red and blue dots in Fig. 12), setting the need for filtering (solid red and blue lines in Fig. 12). In contrast, the proposed algorithm directly outputs a more smooth estimation of the

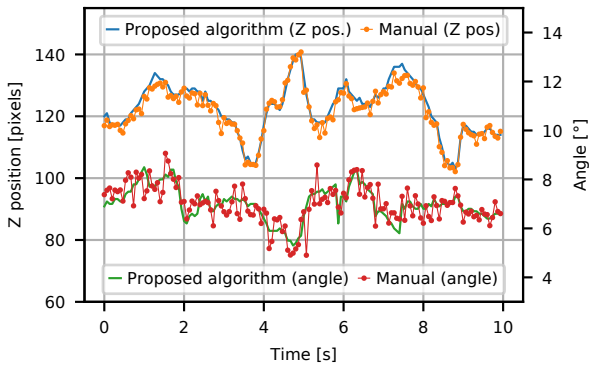

Fig. 11. Comparison between the proposed algorithm (using 15 PW) and the manual annotation for the detection of the deep aponeurosis. The blue and orange lines indicate the z-position indicated by the algoritm and manual annotation, respectively. The green and red lines indicate the corresponding inclination angles.

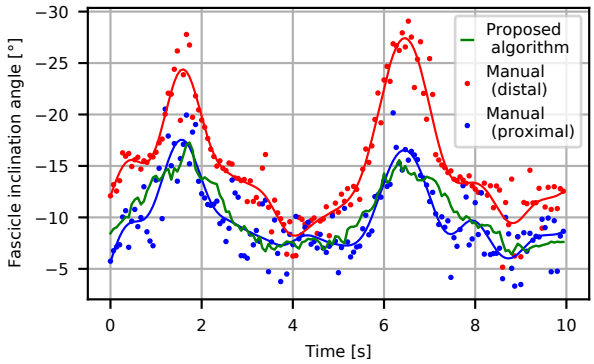

Fig. 12. Comparison between the proposed algorithm (using 15 PW) and expert manual annotation for fascicle inclination angle detection. Red and blue dots indicate the manual annotations for distal and proximal, respectively. The red and blue solid lines are the corresponding filtered version (Butterworth low-pass filter, 5th order, cutoff frequency $= 1\ Hz$). The green line represents the output of the proposed algorithm.

inclination angle, that matches the filtered labels of the proximal area (with a STD of 1.33°). The reason for the algorithm to match the manual annotation on the proximal area is the following: although the algorithm accounts for all the linear structures presented in the ROIs, it gives a higher priority to the brighter fibers with higher energy $E(\alpha)$, which is the case for the proximal fascicles in the selected dataset.

To investigate the performance of the algorithm as a function of the number of PW transmissions, we used multiple compounding schemes (Table I) to produce image sequences with different quality. These sequences were then processed by the proposed algorithm, and the performance statistics were collected.

TABLE I
Compounding schemes

Mode	Tilting angles [°]
PW 1	0
PW 3	$0, \pm(15)$
PW 5	$0, \pm(8.6, 15)$
PW 7	$0, \pm(4.3, 10.7, 15)$
PW 9	$0, \pm(4.3, 8.6, 12.9, 15)$
PW 11	$0, \pm(2.1, 6.4, 10.7, 12.9, 15)$
PW 13	$0, \pm(2.1, 6.4, 8.6, 10.7, 12.9, 15)$
PW 15	$0, \pm(2.1, 4.3, 6.4, 8.6, 10.7, 12.9, 15)$

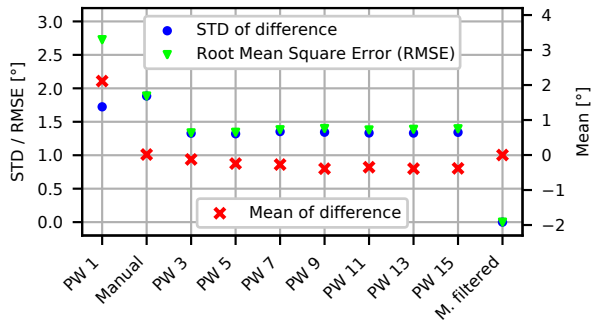

Fig. 13. Mean, STD of the difference and RMSE between multiple methods (manual annotation, automatic annotation for different plane waves) and filtered manually-annotated labels for proximal area (see Fig. 12). Statistics are collected over the selected imaging sequence (150 frames).

Fig. 13 shows the result of the comparison. The proposed algorithm reaches most of its accuracy with only three plane-wave transmissions. The PW 1 mode, composed of a single non-tilted unfocused transmission, is characterized by a high bias (mean $= -2.1°$) and a large variation (STD $= 1.72°$) compared to the reference. After adding two more acquisitions (PW 3) with $\pm 15°$ inclination angles, the accuracy of the angle identification gets significantly improved (mean $= 0.125°$, STD $= 1.32°$). Further increasing the number of transmission does not have a big impact on the performance. Therefore, we can conclude that a simple PW 3 modality can be employed for high frame rate muscle imaging, which allows to relax the minimal hardware requirements (450 acquisition per second) to achieve 150 Hz FR. Combined with the proposed algorithm, PW 3 mode would provide an accuracy of roughly $\pm 2.6°$ for the estimation of the fascicle inclination angle.

V. CONCLUSIONS

This paper presented AEPUS, the first algorithm for the extraction of pennation angles from US images capable of operating with PW datasets. Compared to existing methods, the proposed algorithm does not rely on the edge detection ([9], [10]) or thresholding (for peak extraction [12]) which are sensitive to the quality of US image. Moreover, AEPUS operates on a per-frame basis, without the need to manually select the regions of interest [7] or correct the error accumulated from previous frames [8].

To demonstrate the methodology, we collected US images of slow contractions of medial gastrocnemius muscles, and compared the output of our tool to manual annotations performed by an expert, achieving an accuracy of $\pm 2.6°$. Furthermore, we investigated the tool's performance as a function of the number of plane waves, demonstrating that a PW 3 configuration is sufficient for an accurate tracking of the pennation angle.

Beyond the achieved accuracy, another important property of the proposed algorithm is the minimal number of input parameters. In fact, to calculate the output, only the cropped image and the standard deviation σ for Gaussian kernel (Fig. 9(e)) should be provided.

These results can empower clinicians with a fully automated tool for the estimation of pennation angles with PW imaging. As such, AEPUS can further inspire the clinical translation of plane-wave-based ultrafast US imaging approaches, that appear unique for applications (like CP monitoring) where the fast tracking of motor movements is of critical importance.

We made our Python implementation of the algorithm publicly available and free-to-use under https://github.com/Sergio5714/AEPUS.

ACKNOWLEDGMENT

We thank Michael Rieder (ETH Zürich) for fruitful discussions, Samuel Beuret and Sandra Marcadent (EPFL) for support with the experiments.

REFERENCES

[1] N. J. Cronin and G. Lichtwark, "The use of ultrasound to study muscle–tendon function in human posture and locomotion," *Gait Posture*, vol. 37, no. 3, pp. 305–312, 2013.

[2] G. A. Lichtwark and A. M. Wilson, "Interactions between the human gastrocnemius muscle and the Achilles tendon during incline, level and decline locomotion," *J. Exp. Biol*, vol. 209, no. 21, pp. 4379–4388, 11 2006.

[3] A. Kruse *et al.*, "Muscle and tendon morphology alterations in children and adolescents with mild forms of spastic cerebral palsy," *BMC Pediatr.*, vol. 18, dec 2018.

[4] C. Leitner *et al.*, "A human-centered machine-learning approach for muscle-tendon junction tracking in ultrasound images," *IEEE Trans. Biomed. Eng.*, pp. 1–1, 2021.

[5] B. van Hooren *et al.*, "Ultrasound imaging to assess skeletal muscle architecture during movements: A systematic review of methods, reliability, and challenges," *J. Appl. Physiol.*, vol. 128, pp. 978–999, 4 2020.

[6] N. J. Cronin *et al.*, "Automatic tracking of medial gastrocnemius fascicle length during human locomotion," *J. Appl. Physiol.*, vol. 111, pp. 1491–1496, 11 2011.

[7] G. Q. Zhou and Y. P. Zheng, "Automatic fascicle length estimation on muscle ultrasound images with an orientation-sensitive segmentation," *IEEE Trans. Biomed. Eng.*, vol. 62, pp. 2828–2836, 12 2015.

[8] D. J. Farris and G. A. Lichtwark, "Ultratrack: Software for semi-automated tracking of muscle fascicles in sequences of b-mode ultrasound images," *Comput. Methods Programs Biomed.*, vol. 128, pp. 111–118, 5 2016.

[9] Y. Zhou and Y. P. Zheng, "Estimation of muscle fiber orientation in ultrasound images using revoting hough transform (rvht)," *Ultrasound Med. Biol.*, vol. 34, pp. 1474–1481, 9 2008.

[10] G. Q. Zhou *et al.*, "Automatic measurement of pennation angle and fascicle length of gastrocnemius muscles using real-time ultrasound imaging," *Ultrasonics*, vol. 57, pp. 72–83, 3 2015.

[11] H. Zhao and L. Q. Zhang, "Automatic tracking of muscle fascicles in ultrasound images using localized radon transform," *IEEE Trans. Biomed. Eng.*, vol. 58, pp. 2094–2101, 7 2011.

[12] C. Yuan *et al.*, "Dynamic measurement of pennation angle of gastrocnemius muscles obtained from ultrasound images based on gradient radon transform," *Biomed. Signal Process Control*, vol. 55, p. 101604, 1 2020.

[13] M. Rana *et al.*, "Automated tracking of muscle fascicle orientation in b-mode ultrasound images," *J. Biomech.*, vol. 42, pp. 2068–2073, 9 2009.

[14] C. Leitner *et al.*, "Ultrasound as a tool to study muscle-tendon functions during locomotion: A systematic review of applications," *Sensors*, vol. 19, 10 2019.

[15] M. Tanter and M. Fink, "Ultrafast imaging in biomedical ultrasound," *IEEE Trans. Ultrason. Ferroelectr. Freq. Control*, vol. 61, pp. 102–119, 2014.

[16] G. Montaldo *et al.*, "Coherent plane-wave compounding for very high frame rate ultrasonography and transient elastography," *IEEE Trans. Ultrason. Ferroelectr. Freq. Control*, vol. 56, pp. 489–506, 3 2009.

[17] K. Zuiderveld, "Contrast limited adaptive histogram equalization," *Graphics Gems*, vol. IV, pp. 474–485, 1994.

[18] (2021) Pybf: Python ultrasound beamformer. [Online]. Available: https://github.com/Sergio5714/pybf